Electronic Supplementary Information

for

Cationic Metal-Organic Framework Derived Ruthenium-Copper Nano-alloys in Porous Carbon to Catalytically Boost the Cycle Life for Li-CO_2 Batteries

Zhibin Cheng[#,a,b,*], Ziyuan Wu[#,a], Yiyang Tang[a,b], Xi Fan[a,b], Jindan Zhang[a], Yilong Chen[a], Shengchang Xiang[a], and Zhangjing Zhang[a,b,*]

[a] *Fujian Key Laboratory of Polymer Materials, College of Chemistry and Materials Science, Fujian Normal University, Fuzhou 350007, China. Email: chengzhibin@fjnu.edu.cn, zzhang@fjnu.edu.cn*

[b] *State Key Laboratory of Structural Chemistry, Fujian Institute of Research on the Structure of Matter, Chinese Academy of Sciences, Fuzhou, Fujian, 350002, China*

[#] *These two authors contributed equally to this work.*

Physical Characterizations

Powder X-ray diffraction (XRD) patterns were recorded in the range of 2θ = 5-80° on a desktop X-ray diffractometer (RIGAKU-Miniflex 600) with Cu Kα radiation. X-ray photoelectron spectroscopy (XPS) measurements were performed on a Thermo ESCALAB 250 spectrometer using nonmonochromatic Al Kα X-ray as the excitation source and choosing C 1s (284.8 eV) as the reference line. Thermogravimetric analysis (TGA) was measured at a heating rate of 10 °C min^{-1} using a STA449 C Jupiter thermo gravimetric analyzer (NETZSCH). The Fourier transform infrared (KBr pellets) spectra were recorded in the range of 400-4000 cm^{-1} on a Thermo Nicolet 5700 FT-IR instrument. Nitrogen adsorption/desorption data were recorded at the liquid nitrogen temperature (77 K) using a Micromeritics ASAP 2020 M apparatus. The samples were degassed at 120 °C under vacuum for 12 h prior to the measurement. The specific surface area was calculated using the Brunauer-Emmett-Teller (BET) equation. The pore size distributions were calculated by the nonlocal density functional theory (NL-DFT) model. Scanning electron microscope (SEM) images were obtained with a JSM-6700F field-emission scan electron microscope. Transmission electron microscope (TEM) images were obtained on TECNAI G2F20.

Electrochemical measurements

The lithium-metal chip with a diameter of 15.6 mm and a thickness of 0.25 mm is served as the anode, and the glass fiber diaphragm with a diameter of 18mm is served as the diaphragm. The electrolyte used in this research is 1 M LiTFSI dissolved in the tetraglyme solution. Finally, the 2032 coin-type cells with the holes on the cathode side were taken to fabricate the Li-CO_2 batteries in a glovebox filled with high-purity argon gas, where the moisture and oxygen levels were both kept below 1.0 ppm. The as-prepared coin cells were sealed into the home-made bottle filled with pure CO_2. The Li-CO_2 battery properties were measured in a Neware battery test system (Neware Technology Co.). Before testing, the cells were aged for 24 h. Cyclic voltammetry (CV) and electrochemical impedance spectroscopy (EIS) measurements were performed on CHI604E electrochemical workstation. The CV scan rate was fixed at 0.2 mV s^{-1}, and the voltage range is 2.0-4.5V. The EIS was measured with an applied sinusoidal excitation voltage of 5 mV in the frequency range from 100 kHz to 10 m Hz. The capacity values were normalized by the mass of electrocatalyst in cathodic cathodes. The overpotentials of Li-CO_2 batteries were calculated by voltages difference at the middle of the charge/discharge plateaus. Three-electrode system electrochemical measurements were conducted on an electrochemical workstation (Versa STAT 3F, Princeton Instruments, USA), with a Ag/AgCl electrode and platinum mesh as reference and counter electrodes, respectively. CO_2-saturated 1.0M LiTFSI/TEGDME was used as electrolyte. CO_2 with a flow rate of 20.0 mL ·min^{-1} was through the electrolyte during electrolysis. All the measured potentials were converted to versus Li^+/Li. The LSV scan rate was fixed at 5mV s^{-1}, All the electrochemical data were obtained without iR compensation.

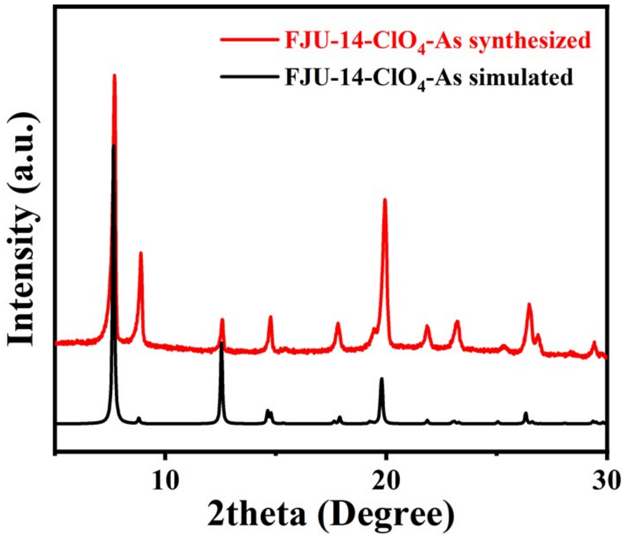

Fig. S1. XRD patterns of the FJU-14-ClO$_4$.

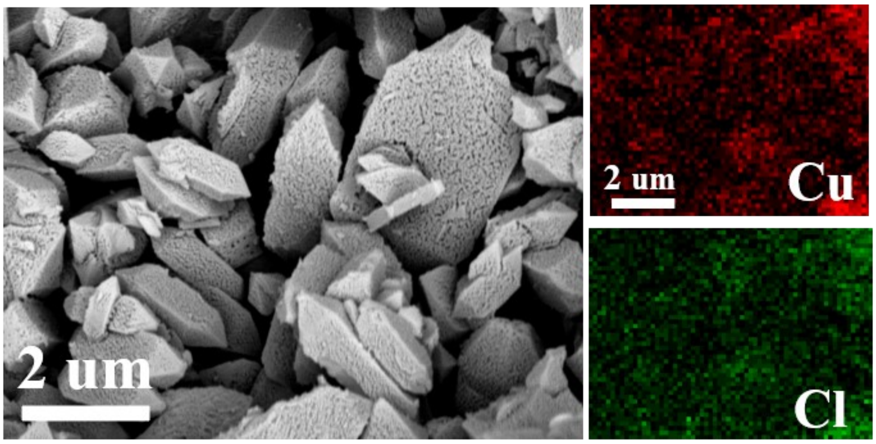

Fig. S2. SEM image of FJU-14-ClO$_4$ and the corresponding elemental mapping images.

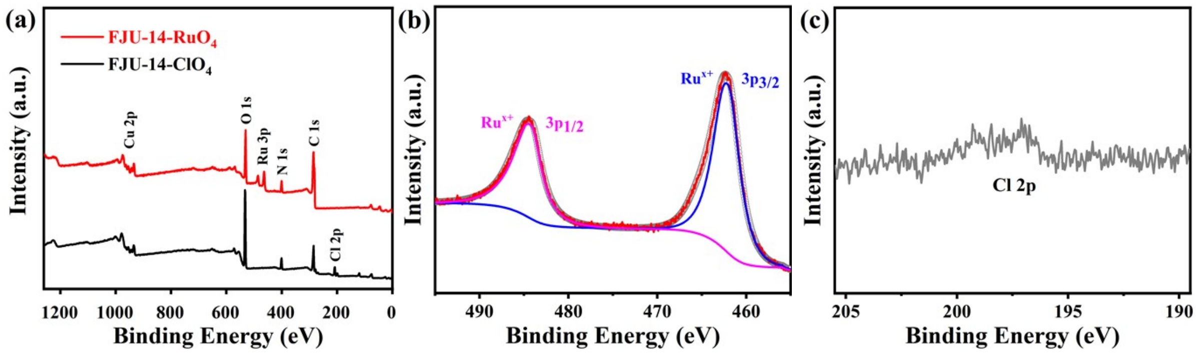

Fig. S3. (a) Full XPS survey spectra for FJU-14-RuO$_4$ and FJU-14-ClO$_4$. High-resolution XPS spectra of (b) Ru 3d and (c) Cl 2p for FJU-14-RuO$_4$.

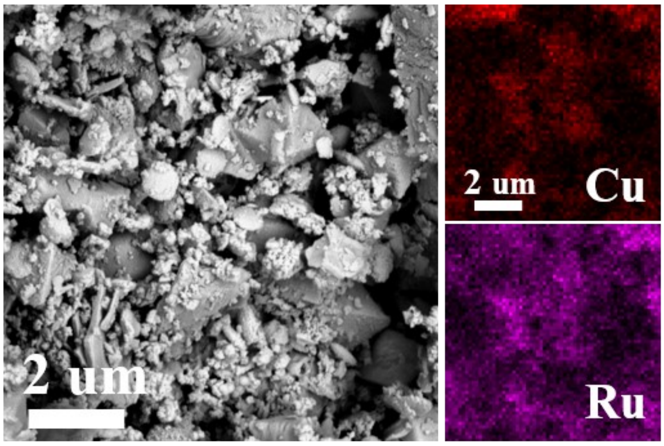

Fig. S4. SEM image of FJU-14-RuO_4 and the corresponding elemental mapping images.

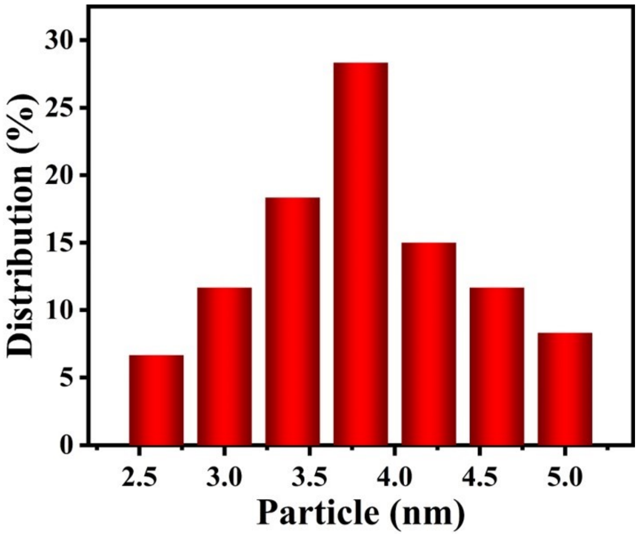

Fig. S5. Particle size distribution of Ru-Cu nanoalloys in Ru-Cu@NPC.

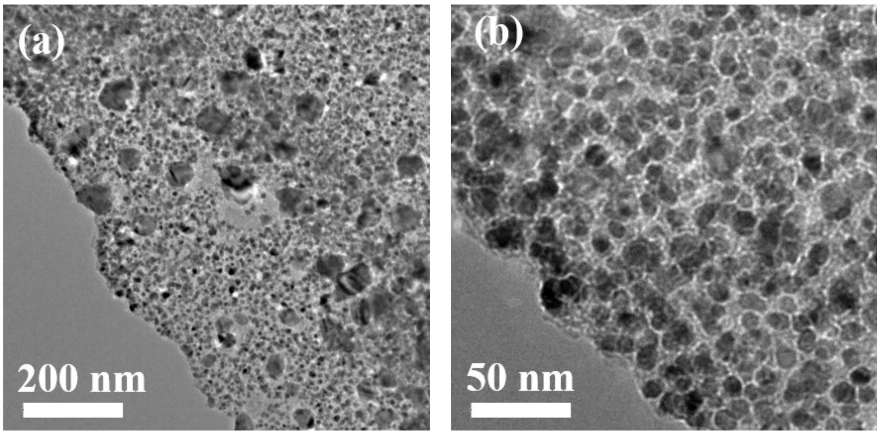

Fig. S6. (a,b) TEM images of Ru@NPC.

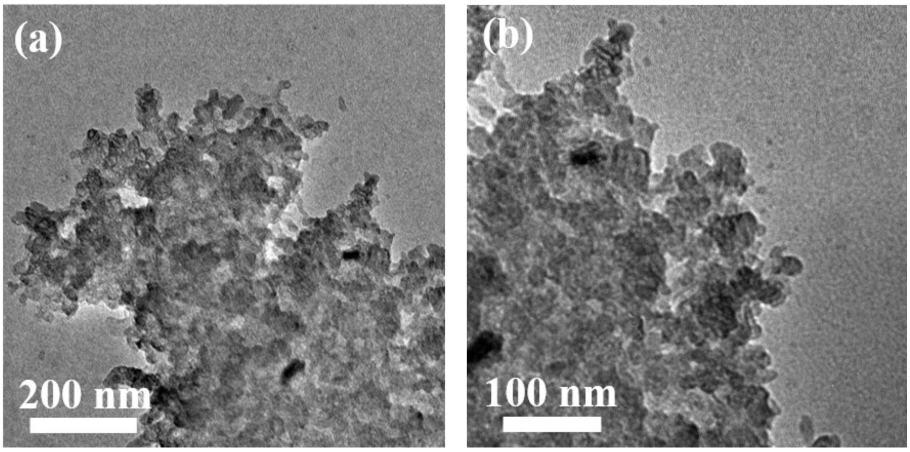

Fig. S7. TEM images of Cu@NPC.

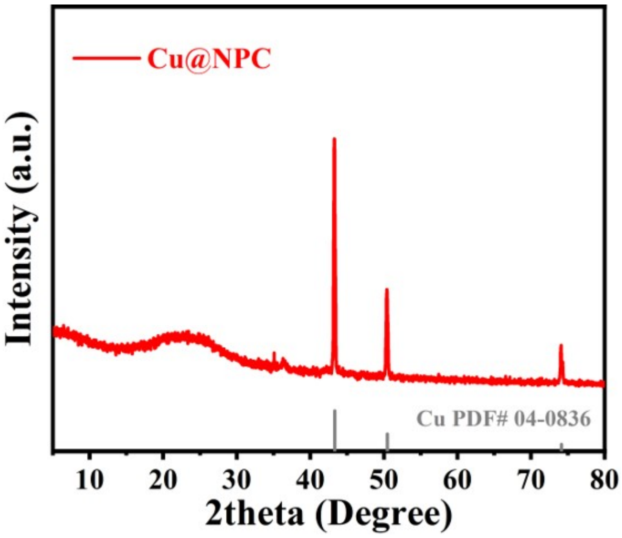

Fig. S8. XRD patterns of the Cu@NPC.

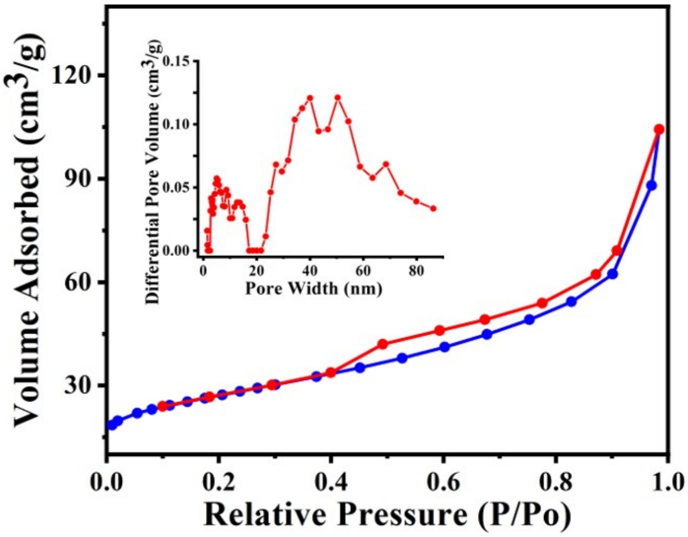

Fig. S9. N_2 adsorption-desorption isotherms and the pore size distribution (the inset) of Ru-Cu@NPC.

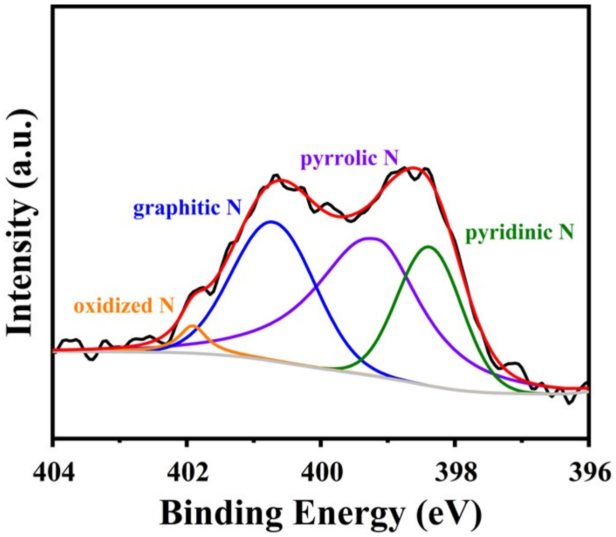

Fig. S10. High-resolution XPS spectra of N 1s for Ru-Cu@NPC.

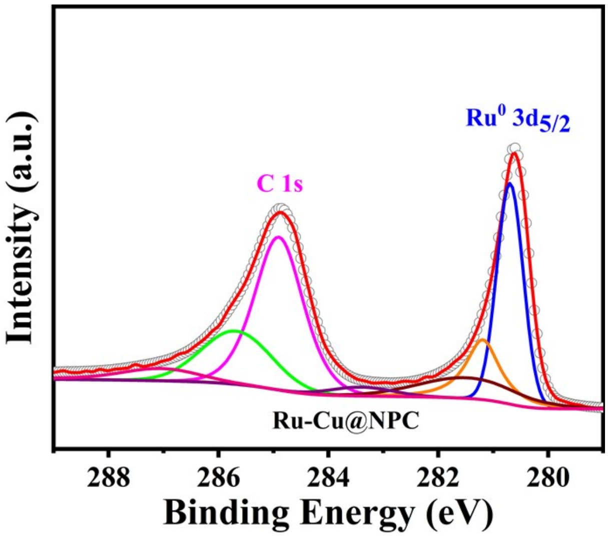

Fig. S11. High-resolution XPS spectra of Ru 3d and C 1s for Ru-Cu@NPC.

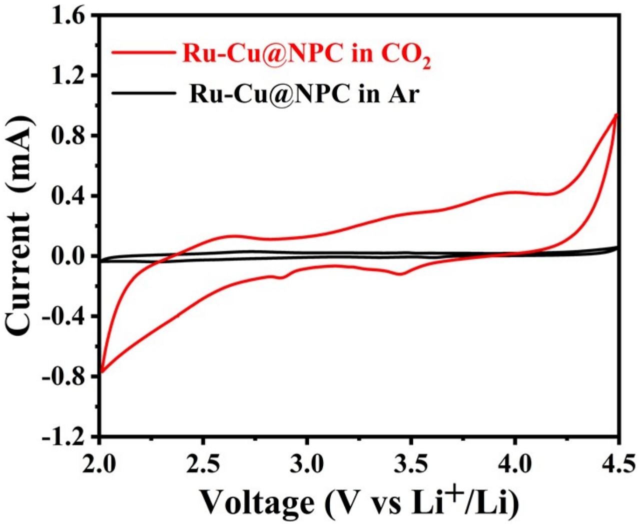

Fig. S12. CV curves of the Li-CO_2 batteries using the Ru-Cu@NPC catalysts at a scanning rate of 0.2 mV s^{-1} in different gas atmospheres.

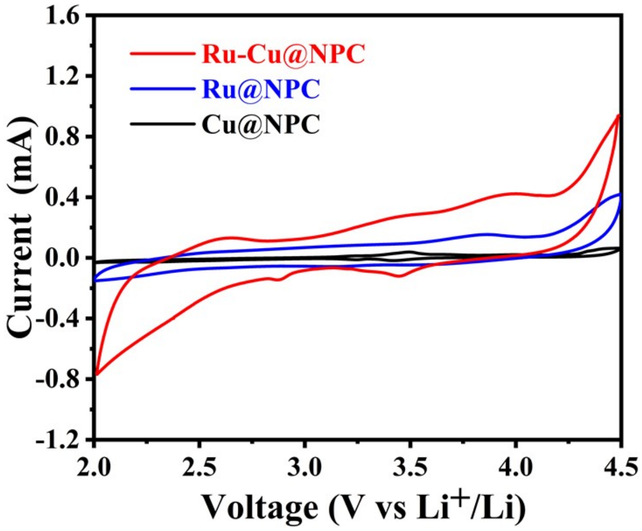

Fig. S13. CV curves of the Li-CO_2 batteries using the Ru-Cu@NPC, Ru@NPC and Cu@NPC catalysts at a scanning rate of 0.2 mV s^{-1}.

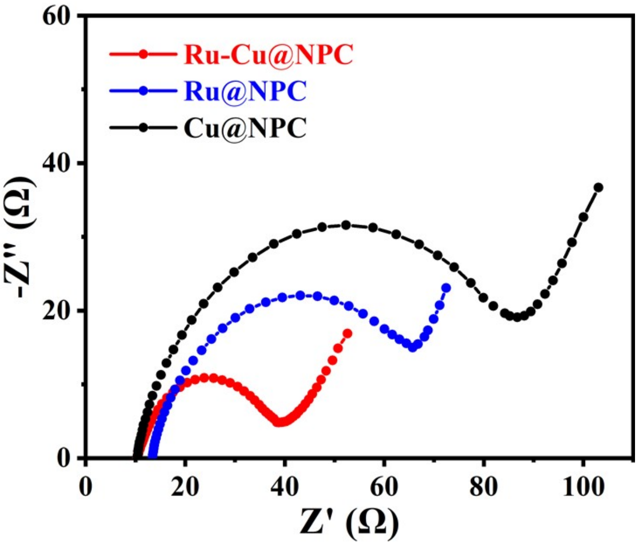

Fig. S14. Impedance spectra of the Li-CO_2 batteries for Ru-Cu@NPC, Ru@NPC, and Cu@NPC cathodes.

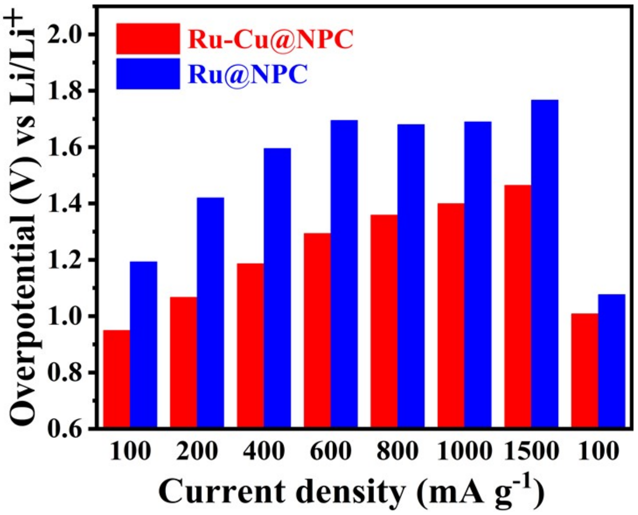

Fig. S15. Battery overpotentials at various current densities based on Ru-Cu@NPC and Ru@NPC electrocatalyst.

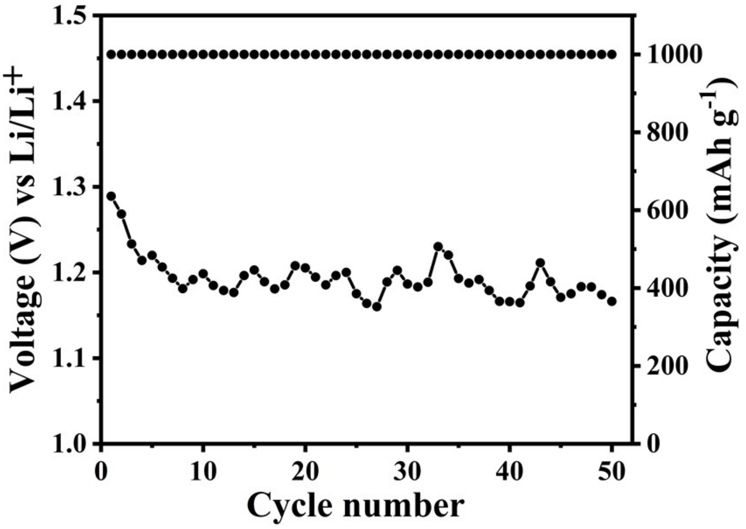

Fig. S16. Cycling performance of Cu@NPC at 400 mA g^{-1}.

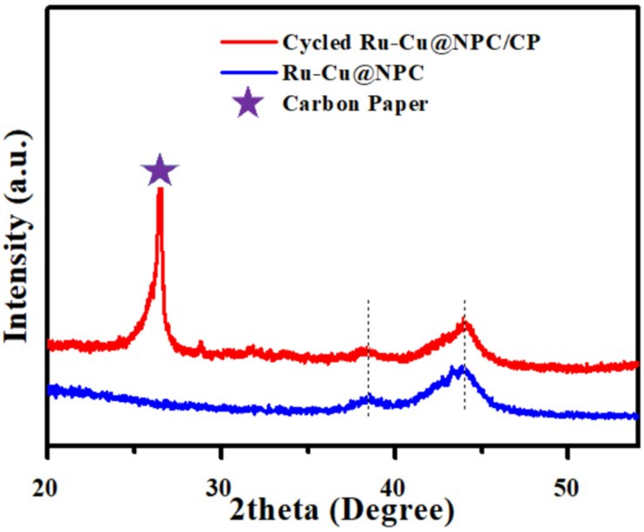

Fig. S17. XRD patterns of Ru-Cu@NPC and cycled Ru-Cu@NPC/CP.

Fig. S18. Two batteries in series power the LED lights in a carbon dioxide atmosphere.

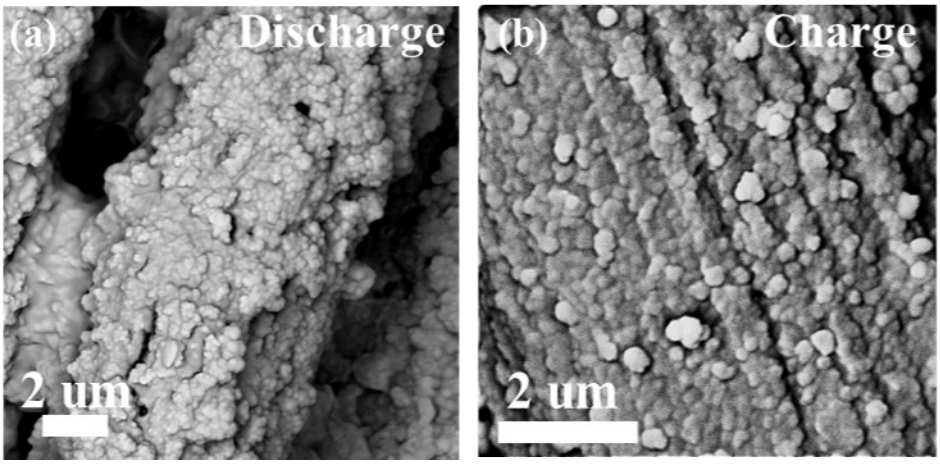

Fig. S19. SEM images of Ru-Cu@NPC cathodes: (a) fully discharge and (b) fully charge states.

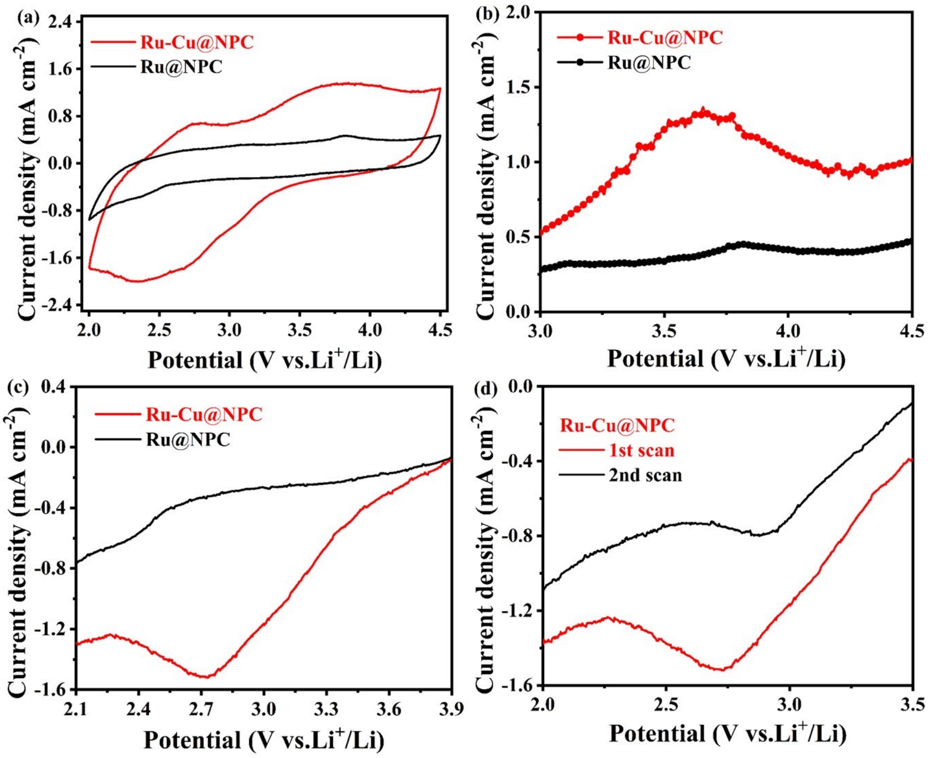

Fig. S20. (a) CV curves at steady states of different electrocatalyst. (b) CO_2ER potential range LSV at steady states of different electrocatalyst. (c) CO_2RR potential range LSV at steady states of different electrocatalyst. (d) Plots of two consecutive LSV scans of Ru-Cu@NPC catalyst.

To further explore Li-CO_2 electrochemistry related to Ru-Cu@NPC catalyst, the CV response of the Ru-Cu@NPC at a constant scanning rate of 5 mV s^{-1} in the 2.0-4.5V range was measured using a three-electrode system (Figure S18a). Obviously, the Ru-Cu@NPC cathode exhibited a higher reduction onset potential and a lower oxidation onset potential, and the peak current densities were larger than those of Ru@NPC, suggesting better catalytic activity of Ru-Cu@NPC. The CO_2 evolution reaction (CO_2ER) and CO_2 reduction reaction (CO_2RR) activities were also measured with a three-electrode system. The much higher anodic current signal and lower onset oxidation potential (3.7V) indicated that the CO_2ER kinetic of Ru-Cu@NPC catalyst was significantly improved (Figure S18b). Meanwhile, the earlier initial potential (2.7V) of the cathodic peak indicated that the interaction of Ru-

Cu@NPC catalyst with dissolved CO_2 molecules greatly promoted CO_2RR (Figure S18c). In addition, after two consecutive LSV scans, the peak current intensity significantly decreased in the second scan (Figure S18d), which could be attributed to the pore-blocking effect of accumulated discharge products.

Table S1. Electrochemical properties of various catalysts in Li-CO$_2$ batteries.

Cathode Catalyst	Charge End Voltage (V)	Overpotential (V)	Discharge capacity (mAh g^{-1})	Cyclic life (cycles)	Ref.
Ru-Cu@NPC	**3.79 (100 mA g^{-1})**	**0.93 (100 mA g^{-1})**	**18204 (100 mA g^{-1})**	**400 (400 mA g^{-1})**	**This work**
CNTs	4.2V (50 mA g^{-1})	-	5786 (100 mA g^{-1})	20 (100 mA g^{-1})	[S1]
Graphene	4.1V (50 mA g^{-1})	1.22 (50 mA g^{-1})	14722 (50 mA g^{-1})	20 (50 mA g^{-1})	[S2]
Ru@Super P	4.0 (100 mA g^{-1})	1.71 (100 mA g^{-1})	8299 (100 mA g^{-1})	80 (100 mA g^{-1})	[S3]
i-Ru$_4$Cu$_1$/CNFs	3.7 (100 mA g^{-1})	0.9 (100 mA g^{-1})	15753 (300 mA g^{-1})	110 (500 mA g^{-1})	[S4]
Ru/ACNF	4.15 (100 mA g^{-1})	1.35 (100 mA g^{-1})	11495 (100 mA g^{-1})	50 (100 mA g^{-1})	[S5]
RuRh allo nanosheets	3.7V (100 mA g^{-1})	1.35 (1 A g^{-1})	9600 (200 mA g^{-1})	180 (1 A g^{-1})	[S6]
Ir NSs-CNFs	3.8 (100 mA g^{-1})	1.05 (100 mA g^{-1})	7666.7 (166 mA g^{-1})	400 (500 mA g^{-1})	[S7]
Fe-ISA/N,S-HG	3.95 (100 mA g^{-1})	1.17 (100 mA g^{-1})	23174 (100 mA g^{-1})	100 (1 A g^{-1})	[S8]
Cu-NG	3.03 (200 mA g^{-1})	0.77 (200 mA g^{-1})	14864 (200 mA g^{-1})	50 (200 mA g^{-1})	[S9]
MoS$_2$ nanoflakes	3.6 (100 mA g^{-1})	0.7 (100 mA g^{-1})	60000 (100 mA g^{-1})	500 (500 mA cm^{-1})	[S10]
SA Ru-Co3O4/CC	-	1.05 (100 mA g^{-1})	16510 (300 mA g^{-1})	251 (200 mA g^{-1})	[S11]
TGD-1000	-	1.12 (100 mA g^{-1})	69965 (500 mA g^{-1})	600 (1 A g^{-1})	[S12]
W$_2$C-CNTs	3.22 (100 mA g^{-1})	-	10632 (100 mA g^{-1})	75 (200 mA g^{-1})	[S13]
COF-Ru@CNT	2.73 (200 mA g^{-1})	1.24 (200 mA g^{-1})	27348 (200 mA g^{-1})	150 (400 mA g^{-1})	[S14]
BN-hG	3.9V (100 mA g^{-1})	-	16033 (300 mA g^{-1})	200 (1 A g^{-1})	[S15]

References

[S1] X. Zhang, Q. Zhang, Z. Zhang, Y. Chen, Z. Xie, J. Wei, Z. Zhou, *Chem. Commun.* **2015**, *51*, 14636.

[S2] Z. Zhang, Q. Zhang, Y. Chen, J. Bao, X. Zhou, Z. Xie, J. Wei, Z. Zhou, *Angew. Chem. Int. Ed.* **2015**, *54*, 6550.

[S3] S. Yang, Y. Qiao, P. He, Y. Liu, Z. Cheng, J.-j. Zhu, H. Zhou, *Energy Environ. Sci.* **2017**, *10*, 972.

[S4] Y. Jin, F. Chen, J. Wang, R. L. Johnston, *Chem. Eng. J.* **2019**, *375*.

[S5] Y. Qiao, S. Xu, Y. Liu, J. Dai, H. Xie, Y. Yao, X. Mu, C. Chen, D. J. Kline, E. M. Hitz, B. Liu, J. Song, P. He, M. R. Zachariah, L. Hu, *Energy Environ. Sci.* **2019**, *12*, 1100.

[S6] Y. Xing, K. Wang, N. Li, D. Su, W.-T. Wong, B. Huang, S. Guo, *Matter* **2020**, *2*, 1494.

[S7] Y. Xing, Y. Yang, D. Li, M. Luo, N. Chen, Y. Ye, J. Qian, L. Li, D. Yang, F. Wu, R. Chen, S. Guo, *Adv. Mater.* **2018**, *30*, e1803124.

[S8] C. Hu, L. Gong, Y. Xiao, Y. Yuan, N. M. Bedford, Z. Xia, L. Ma, T. Wu, Y. Lin, J. W. Connell, R. Shahbazian-Yassar, J. Lu, K. Amine, L. Dai, *Adv. Mater.* **2020**, *32*, e1907436.

[S9] Z. Zhang, Z. Zhang, P. Liu, Y. Xie, K. Cao, Z. Zhou, *J. Mater. Chem. A* **2018**, *6*, 3218.

[S10] A. Ahmadiparidari, R. E. Warburton, L. Majidi, M. Asadi, A. Chamaani, J. R. Jokisaari, S. Rastegar, Z. Hemmat, B. Sayahpour, R. S. Assary, B. Narayanan, P. Abbasi, P. C. Redfern, A. Ngo, M. Voros, J. Greeley, R. Klie, L. A. Curtiss, A. Salehi-Khojin, *Adv. Mater.* **2019**, *31*, 1902518.

[S11] Z. Lian, Y. Lu, C. Wang, X. Zhu, S. Ma, Z. Li, Q. Liu, S. Zang, *Adv. Sci.* **2021**, *8*, e2102550.

[S12] F. Ye, L. Gong, Y. Long, S. N. Talapaneni, L. Zhang, Y. Xiao, D. Liu, C. Hu, L. Dai, *Adv. Energy Mater.* **2021**, *11*.

[S13] X. Zhang, T. Wang, Y. Yang, X. Zhang, Z. Lu, J. Wang, C. Sun, Y. Diao, X. Wang, J. Yao, *ACS Energy Lett.* **2021**, *6*, 3503.

[S14] X. Li, H. Wang, Z. Chen, H. S. Xu, W. Yu, C. Liu, X. Wang, K. Zhang, K. Xie, K. P. Loh, *Adv. Mater.* **2019**, *31*, 1905879.

[S15] Y. L. Long Qie, John W. Connell, Jiantie Xu, and Liming Dai, *Angew. Chem. Int. Ed.* **2017**, *129*, 7074.